Supporting Information for "Observations of the size distribution of frazil ice in an Ice Shelf Water plume"

Eamon K. Frazer[1], Pat J. Langhorne[1], Greg H. Leonard[2], Natalie J. Robinson[3], Dániel Schumayer[1,4]

[1]Department of Physics, University of Otago, Dunedin, New Zealand
[2]School of Surveying, University of Otago, Dunedin, New Zealand
[3]National Institute of Water and Atmospheric Research, Wellington, New Zealand
[4]The Dodd-Walls Centre for Photonic and Quantum Technologies, Dunedin, New Zealand

Contents of this file

Description of the AZFP

The AZFP profiles the water column by pulsing acoustic waves at four frequencies (125 kHz, 200 kHz, 455 kHz, and 769 kHz) using four separate monostatic transducers and receivers. The acoustic backscatter is recorded by the instrument and converted to a volume backscatter strength. Ten profiles were collected at each sampling interval and then averaged. Samples were undertaken at 1 minute intervals. The ASL Matlab Toolbox (version 1.1) was used to convert raw instrument counts to acoustic volume backscattering strength, S_v, related to the back-scattering cross section, $\Sigma_{\rm bs}^{\rm obs}$.

The S_v data are taken as a time series at fixed ranges in each deployment, such that they remain roughly equidistant from the ice-ocean interface over time. Data are measured in 0.1 m vertical cells, then spatially averaged over 0.5 m centered on the depth specified in the analysis. The resulting spatially-averaged time series is smoothed using MATLAB's `rlowess` algorithm, a 1st degree polynomial model with linear least square fitting. This process is repeated for all depths of interest in the water column, from the ice-ocean interface down to ≈2m from the AZFP. This range excludes the bulk of the ice layer and the portion of the water column affected by the near-field interference of the sonar.

Further details of the instrumentation and its mode of deployment are available in Kungl et al. (2020), Frazer (2019) and in the metadata files of Robinson et al. (2020b).

Details of data analysis

An overview of the data processing is shown in Figure S1.

The total back-scattering cross-section, $\Sigma_{\rm bs}^{\rm th}(\nu)$, at frequency ν for a dilute population of scatterers with random diameter D can be modeled by

$$\Sigma_{\rm bs}^{\rm th}(\nu) = N \int g(D)\, \sigma_{\rm bs}(\nu, D)\, dD, \qquad (1)$$

where $\Sigma_{\rm bs}^{\rm th}(\nu)$ is the ratio of back-scattered intensity from a unit volume of $1{\rm m}^3$ to the intensity of the incident plane wave (referenced to 1m), N is the number density of scatterers, $\sigma_{\rm bs}$ is the scattering cross-section of a single obstacle, and g is a probability distribution of scatterers' diameter (Marko & Jasek, 2010). Below we model g and $\sigma_{\rm bs}$, and identify the left-hand side of this equation with the measured back-scattering cross-section $\Sigma_{\rm bs}^{\rm obs}(\nu)$, noting that

$$S^{\rm obs} = 10\log_{10}(\Sigma_{\rm bs}^{\rm obs}) \quad \text{and} \quad S^{\rm th} = 10\log_{10}(\Sigma_{\rm bs}^{\rm th}).$$

Recent observations (Marko et al., 2015; McFarlane et al., 2017, 2019; Schneck et al., 2019) and theoretical considerations (Crow & Shimizu, 1988) recommend choosing a log-normal distribution for g. This probability distribution is governed by a location and a scale parameter, μ and σ. Parameters μ and σ are the mean and standard deviation of the transformed random variable $\ln(D)$, where ln() denotes the natural logarithm. The physically important statistical moments of D are

$$\begin{aligned} \text{median}(D) &= \exp(\mu), \\ \text{mean}(D) &= \exp(\mu + \tfrac{1}{2}\sigma^2), \\ \text{mode}(D) &= \exp(\mu - \sigma^2), \quad \text{and} \\ \text{variance}(D) &= \left[\exp(\sigma^2) - 1\right] \exp(2\mu + \sigma^2) \end{aligned}$$

Assuming low scatterer number and a uniformly random orientation of crystals, we have provided an analytic expression for the back-scattering cross-section $\sigma_{\rm bs}$ of an individual crystal modeled as an oblate spheroid (Kungl et al., 2020).

Although g depends on yet unknown parameters, and $\sigma_{\rm bs}$ is expressed in terms of a random variable D and known frequencies, the integral (1) can be determined either analytically or numerically for any given set of $\{\mu, \sigma, N\}$. Thus there are three unknown quantities and four measurement channels at a given depth and given time, hence the mathematical problem is over-determined assuming perfect observation. However, since observed data are encumbered with noise from different sources, it is more natural to re-interpret the task of determining $\{\mu, \sigma, N\}$ as an optimization problem. We seek the parameter values that optimally approximate the observed back-scattering cross-sections, $\Sigma_{\rm bs}^{\rm obs}$, provided by observation. The goodness-of-fit is measured by the standard residual sum of squares

$$R = \sum_{i=1}^{4} \left[S^{\rm th}(\nu_i) - S^{\rm obs}(\nu_i) \right]^2.$$

In order to limit R to $\sim$ 1dB (similar to the uncertainty of the instrument) some constraints are placed on the parameter space to avoid non-physical solutions. An upper bound is put on the total fractional ice volume, F, defined as the volume of ice per cubic meter of ocean

$$F = N \int g(D)\, V(D, \tau)\, dD = \frac{\pi}{6}\, N\tau \exp\left(3\mu + \tfrac{9}{2}\sigma^2\right), \qquad (2)$$

0094-8276/20/$5.00

where $V(D,\tau) = \frac{\pi}{6}D^3\tau$ is the volume of a single oblate spheroidal crystal of diameter D and thickness ratio τ. In this work we use $\tau = 1/30$ (Dempsey et al., 2010; McFarlane et al., 2012, 2014; Kungl et al., 2020) and employed the numerical constraint, $F < 10^{-1}$. This constraint is quite permissive, much higher than expected values in the ocean (Penrose et al., 1994). For the nonlinear constrained optimization we used Matlab's built-in interior-point algorithm, `fmincon`. The optimization procedure terminates if

1. R has reached its minimum at a tolerance of 10^{-6}, and
2. F does not change by more than 10^{-12}.

The same process (see Figure S1) is repeated for the entire time-series.

Notes on data filtering

Removal of data with $S^{\text{obs}} > -45\,\text{dB}$ value can be justified because such signals are present at all frequencies indicating large scatterers. Most likely signals are from the bottom of the sub-ice platelet layer or perhaps due to occasional large marine life.

The bimodality of the distribution of S_v in Figure 2a of the main manuscript suggested that there could be two (or more) distinct cohort of scatterers. That histogram represents the 200 kHz channel of the dataset taken 5–9 November 2017. Therefore we chose to fit two Gaussian distributions to this histogram and obtained mean and standard deviations of $(\mu_1, \sigma_1) = (-101.00, 10.96)\,\text{dB}$ and $(\mu_2, \sigma_2) = (-75.00, 7.23)\,\text{dB}$. From these parameters we select a cut-off value in the range $(-90, -83)\,\text{dB}$.

Unlike the oblate spheroidal scattering model, or the optimization algorithm, this choice was heuristic. Consequently we repeated the optimization algorithm calculation for a few cut-off values in this range. These optimization runs all led to similar $\{\mu_{10}, \sigma, N\}$ results. Hence we concluded that the optimization was not sensitive to the precise value of the cut-off value of $-85\,\text{dB}$. It is apparent from Figure 2b-d of the main text that the blue and orange data points, determined by their S_v values, do represent physically distinct groups of $\{\mu_{10}, \sigma, N\}$ parameters and the cohort colored blue corresponds to very large number of extremely small particles, which –on physical grounds– we managed to exclude from any analysis by imposing the cut-off values on the S_v data.

Two remarks are due here.

(i) In selecting the 200 kHz channel for determining the cut-off value we considered two counteracting arguments. First, we wanted to select a channel which is the 'loudest', i.e., has the highest frequency, as it picks up more features in the insonified volume. On the other hand we wanted a channel which is insensitive against details our model does not contain. This second consideration means that we wish all scatterers to scatter within the Rayleigh regime, i.e., the frequency cannot be too high. Thus we opt for the 200 kHz channel.

(ii) While not all deployments and all channels show such clear bimodality, we checked the 200 kHz channel of other deployments and fitted a mixture of two Gaussians on these histograms too. Those transition ranges did contain the $-85\,\text{dB}$ value.

Comparison with salt water laboratory studies

Figure S2 shows the log-normal population density function using the mean parameter values at 15 mBSL in 2017 in comparison to the frazil ice distributions in saline water of 35 ppt found by Schneck et al. (2019). Distribution mean, standard deviation, and mode are shown. The larger standard deviation of the present work probably arises because we are unable to separate individual crystals from flocs as has been done by Schneck et al. (2019).

References

Crow, E. L., & Shimizu, K. (1988). *Lognormal distributions: theory and applications* (E. L. Crow & K. Shimizu, Eds.). New York: M. Dekker.

Dempsey, D. E., Langhorne, P. J., Robinson, N. J., Williams, M. J. M., Haskell, T. G., & Frew, R. D. (2010, jan). Observation and modeling of platelet ice fabric in McMurdo Sound, Antarctica. *Journal of Geophysical Research*, *115*(C1). doi: 10.1029/2008jc005264

Frazer, E. (2019). *Characterising Frazil Ice Populations using Acoustic Techniques* (M. Sc. thesis). University of Otago.

Kungl, A. F., Schumayer, D., Frazer, E. K., Langhorne, P. J., & Leonard, G. H. (2020). An oblate spheroidal model for multi-frequency acoustic back-scattering of frazil ice. *Cold Regions Science and Technology*, *177*, 103122. doi: https://doi.org/10.1016/j.coldregions.2020.103122

Marko, J. R., & Jasek, M. (2010). Sonar detection and measurements of ice in a freezing river I: Methods and data characteristics. *Cold Regions Science and Technology*, *63*(3), 121–134.

Marko, J. R., Jasek, M., & Topham, D. R. (2015, feb). Multifrequency analyses of 2011–2012 Peace River SWIPS frazil backscattering data. *Cold Regions Science and Technology*, *110*, 102–119. doi: 10.1016/j.coldregions.2014.11.006

McFarlane, V., Loewen, M., & Hicks, F. (2012). Laboratory experiments to determine frazil ice properties. In *Proceedings of the Annual General Conference of the Canadian Society of Civil Engineers, Edmonton, Alberta, Canada, June* (Vol. 6).

McFarlane, V., Loewen, M., & Hicks, F. (2014, oct). Laboratory measurements of the rise velocity of frazil ice particles. *Cold Regions Science and Technology*, *106-107*, 120–130. doi: 10.1016/j.coldregions.2014.06.009

McFarlane, V., Loewen, M., & Hicks, F. (2017, October). Measurements of the size distribution of frazil ice particles in three Alberta rivers. *Cold Regions Science and Technology*, *142*, 100–117. doi: 10.1016/j.coldregions.2017.08.001

McFarlane, V., Loewen, M., & Hicks, F. (2019). Field measurements of suspended frazil ice. part ii: Observations and analyses of frazil ice properties during the principal and residual supercooling phases. *Cold Regions Science and Technology*, *165*, 102796. doi: https://doi.org/10.1016/j.coldregions.2019.102796

Penrose, J. D., Conde, M., & Pauly, T. J. (1994). Acoustic detection of ice crystals in Antarctic waters. *Journal of Geophysical Research*, *99*(C6), 12573. doi: 10.1029/93jc03507

Robinson, N. J., Leonard, G., Frazer, E., Langhorne, P., Grant, B., Stewart, C., & De Joux, P. (2020b). Temperature, salinity and acoustic backscatter observations and tidal model output in McMurdo Sound, Antarctica in 2016 and 2017. In *Pangaea Data Archiving.* Alfred Wegener Institute, Helmholtz Centre for Polar and Marine Research. doi: pending

Schneck, C. C., Ghobrial, T. R., & Loewen, M. R. (2019). Laboratory study of the properties of frazil ice particles and flocs in water of different salinities. *The Cryosphere*, *13*(10), 2751–2769. doi: 10.5194/tc-13-2751-2019

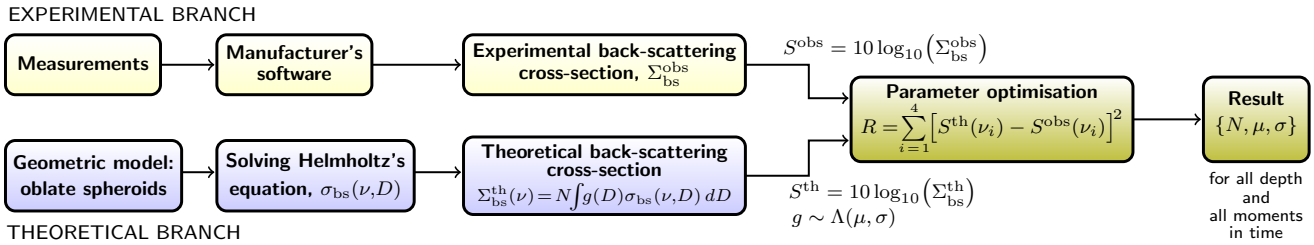

Figure S1. The flow diagram shows how the experimental and data preparation and the theoretical modeling are combined in a classical optimization process to obtain estimates of $\{N, \mu, \sigma\}$. Here N denotes the number of frazil crystals in the insonified volume at a given depth and a fixed moment in time. Parameters μ and σ characterize the log-normal probability distribution $g \sim \Lambda(\mu, \sigma)$ describing the likelihood observing an oblate spheroid of size D.

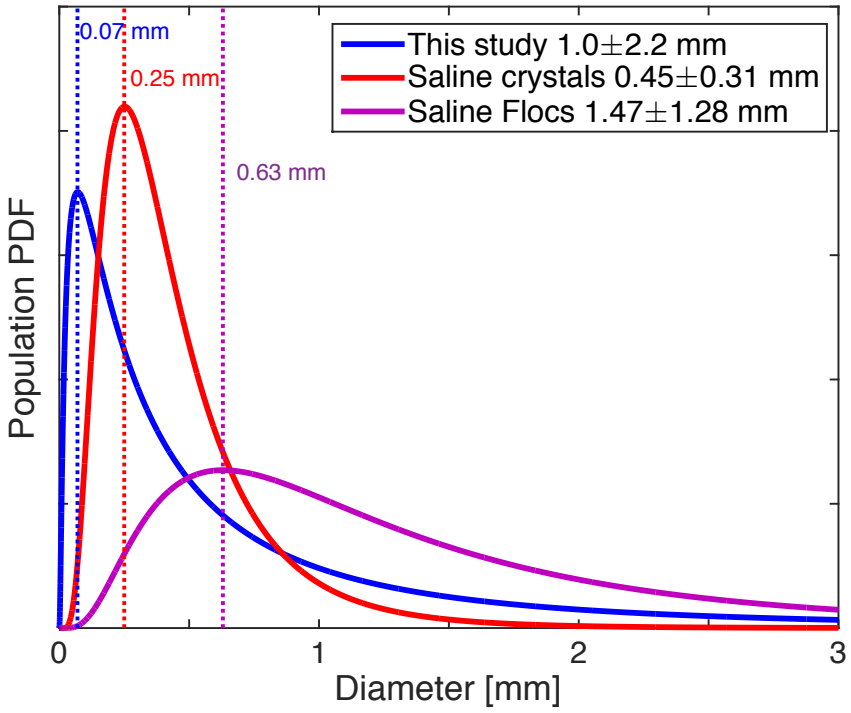

Figure S2. Comparison of present distribution (in blue) with that of salt water experiments at 35 ppt of Schneck et al. (2019), with individual frazil ice crystals in red and frazil flocs in magenta. The arithmetic mean and standard deviation of each distribution is shown in the legend. The modes (the most likely values of the distribution) are shown by vertical dotted lines and color-coded.